SUPPORTING INFORMATION

Lanthanide Functionalized Covalent Triazine Framework as Physiological Molecular Thermometer

Parviz Gohari Derakhshandeh,† Sara Abednatanzi,† Laurens Bourda, Sasanka Dalapati, Anatolii Abalymov, Maria Meledina, Ying-Ya Liu, Andre G. Skirtach, Kristof Van Hecke , Anna M. Kaczmarek, Pascal Van Der Voort**

Materials and Methods. All reagents were purchased from commercial sources and used without further purification. Fourier Transform Infrared Spectroscopy (FT-IR) in the region 4000-650 cm^{-1} was performed with a Thermo Nicolet 6700 FTIR spectrometer equipped with a nitrogen-cooled MCT detector and a KBr beam splitter. X-ray powder diffraction (XRPD) patterns were obtained on a Thermo Scientific ARL X'Tra diffractometer, operated at 40 kV, 30 mA using Cu-Kα radiation (λ = 1.5406 Å). Nitrogen adsorption-desorption isotherms were obtained using a Belsorp Mini apparatus measured at 77 K. Elemental analyses (C, H, N and O) were carried out on a Thermo Scientific Flash 2000 CHNS-O analyzer equipped with a TCD detector. Thermogravimetric analysis (TGA) was carried out on a Neetzsch STA-449F3 Jupiter simultaneous TG-DSC analyzer within a temperature range of 20-1000 °C, under air atmosphere and at a heating rate of 10 °C/min. The morphology of the sample was observed using field–emission scanning electron microscope (FE-SEM) FEI Nova NanoSEM 450. High angle annular dark-field scanning transmission electron microscopy (HAADF STEM) images were collected using a JEOL JEM-2200FS transmission electron microscope with a post-sample Cs corrector and an accelerating voltage of 200 kV. For the sample preparation, the materials were dispersed in isopropanol by using an ultrasonic bath for 15 minutes. A copper support TEM grid (200 mesh) was dipped in the dispersion and air-dried before measurement. Annular dark-field

scanning transmission electron microscopy (ADF-STEM) imaging was performed using an FEI Titan electron microscope operated at an accelerating voltage of 300 kV and equipped with a spherical aberration corrector unit. The samples were prepared by dispersing in ethanol and dropping onto the carbon coated TEM copper grid. The ^{13}C MAS NMR spectra were collected at 125.69 MHz using a 4 mm MAS NMR probe with a spinning rate of 8 kHz and a pulse width of 2.5 μs for a π/4 pulse, and 1800-2700 scans were gathered with a 4 s recycle delay. The luminescence of solid samples was studied. Solid powdered samples were put between quartz plates (Starna cuvettes for powdered samples, type 20/C/Q/0.2). Colloidal suspensions were measured in quartz cuvettes with a path length of 10 mm. Luminescence measurements were performed on an Edinburgh Instruments FLSP920 UV-vis-NIR spectrometer setup. A 450W xenon lamp was used as the steady state excitation source. Luminescence decay times were recorded using a 60W pulsed Xe lamp, operating at a frequency of 100 Hz. A Hamamatsu R928P photomultiplier tube was used to detect the emission signals in the near UV to visible range. All of the luminescence measurements were recorded at room temperature unless indicated otherwise. The temperature-dependent luminescent measurements of the powder samples were measured using an ARS CS202-DMX-1SS closed cycle cryostat (4K – 800 K) controlled with a Lake Shore Model 336 temperature controller. The temperature-dependent luminescent measurements of the CTF material suspended in water were performed using a Julabo refrigerated and heating F-25 circulator in a temperature range of 283.15 K to 323.15 K with steps of 5 K, which was circulating through the cuvette holder supplied by the Edinburgh Instruments. All emission spectra in the manuscript have been corrected for detector response. The luminescence decay curves of the samples were measured when excited into the maximum of the broad ligand band and monitored at the appropriate wavelength (strongest peak of the

given lanthanide). All of the decay curves could be well fitted using either a single exponential function or biexponential function.

$$I = A\exp\left(-\frac{t}{\tau}\right)$$

$$I = A_1\exp\left(-\frac{t}{\tau_1}\right) + A_2\exp\left(-\frac{t}{\tau_2}\right)$$

Where I represents the luminescence intensity of a transition and A, A_1 and A_2 are constants, t is time and τ, τ_1 and τ_2 are the luminescence lifetimes. The temperature-measurements were performed using an ARS closed cycle cryostat at a temperature range between 200 – 340 K. For the conversion of intensity into temperature the thermometric parameter Δ was employed. Here, $\alpha = W_0/W_R$ is the ratio between the nonradiative (W_0 at T = 0 K) and radiative (W_R) rates, ΔE is the activation energy for the nonradiative channel, and Δ_0 is the thermometric parameter at T = 0 K.

$$\Delta = \frac{I1}{I2} = \frac{\Delta_0}{1 + \alpha\exp\left(-\frac{\Delta E}{k_B T}\right)}$$

The relative temperature sensitivity S_r was calculated using the following equation:

$$S_r = 100\% \times \left|\frac{1}{\Delta}\frac{\partial\Delta}{\partial T}\right|$$

S_r indicates the relative change of the thermometric parameter per degree of temperature change (% K^{-1}). S_r is independent of the nature of the thermometer and allows direct and quantitative comparison of different materials. All calculations were carried out employing the TeSen software.[1] To fully evaluate the performance of the thermometer additionally the uncertainty was

calculated as well as the reproducibility after several cycles. The temperature uncertainty δT is one of the important parameters in assessment of the performance of the desired thermometer. Calculation of the δT can be determined with the following equation:

$$\delta T = \frac{1}{S_r}\frac{\delta\Delta}{\Delta}$$

The performance stability of thermometers is estimated by cycling the temperature in the given temperature interval ensuring that the thermometer reach the thermal equilibrium for each measurement and it can be given with:

$$R = 1 - \frac{\max\left(|\Delta_c - \Delta_i|\right)}{\Delta_c}$$

where the Δ_c is the mean thermometric parameter extracted from the calibration curve and Δ_i is value of each thermometric parameter measurement.

Cell cultivation. NHDF Fibroblastic cell of NHDF cells were cultured in DMEM (Cat. No. D5546) supplemented with 10% FBS, 2 mM glutamine, and 100 μg/ml penicillin/streptomycin. The media were replaced every 3 days, and the cells were maintained in a humidified incubator at 5% CO_2 and 37 °C with 5% CO_2 (Innova CO-170, New Brunswick Scientific).

Cell Viability. NHDF cells were seeded into 96-well cell culture plates at a cell density of 10×10^4 /well. After 24 h cultivation, particles from 0.001 mg/well till 1 mg/well were placed into the plate in the culture medium and incubated overnight at 37 °C under 5% CO_2. Subsequently, cells were incubated (Innova CO-170, New Brunswick Scientific) at 37 °C for 4 h, together with 10 μL of fluorescence dye was added to each well (Alamar Blue, Sigma-Aldrich). In the last step fluorescent (540/610 nm) intensity was measured by a spectrophotometer (Synergy H1Multi-Mode Reader).

Fluorescence microscopy: To visualize viable cells a Nikon TI (Nikon, Japan) fluorescence microscope with the following objective 10X and appropriate filters was used. After 1 days of incubation with Bipy-CTF particles, cell layers were then stained with calcein AM. Cells were incubated with a medium containing 0.1 mM of the reagent for 10 min at RT.

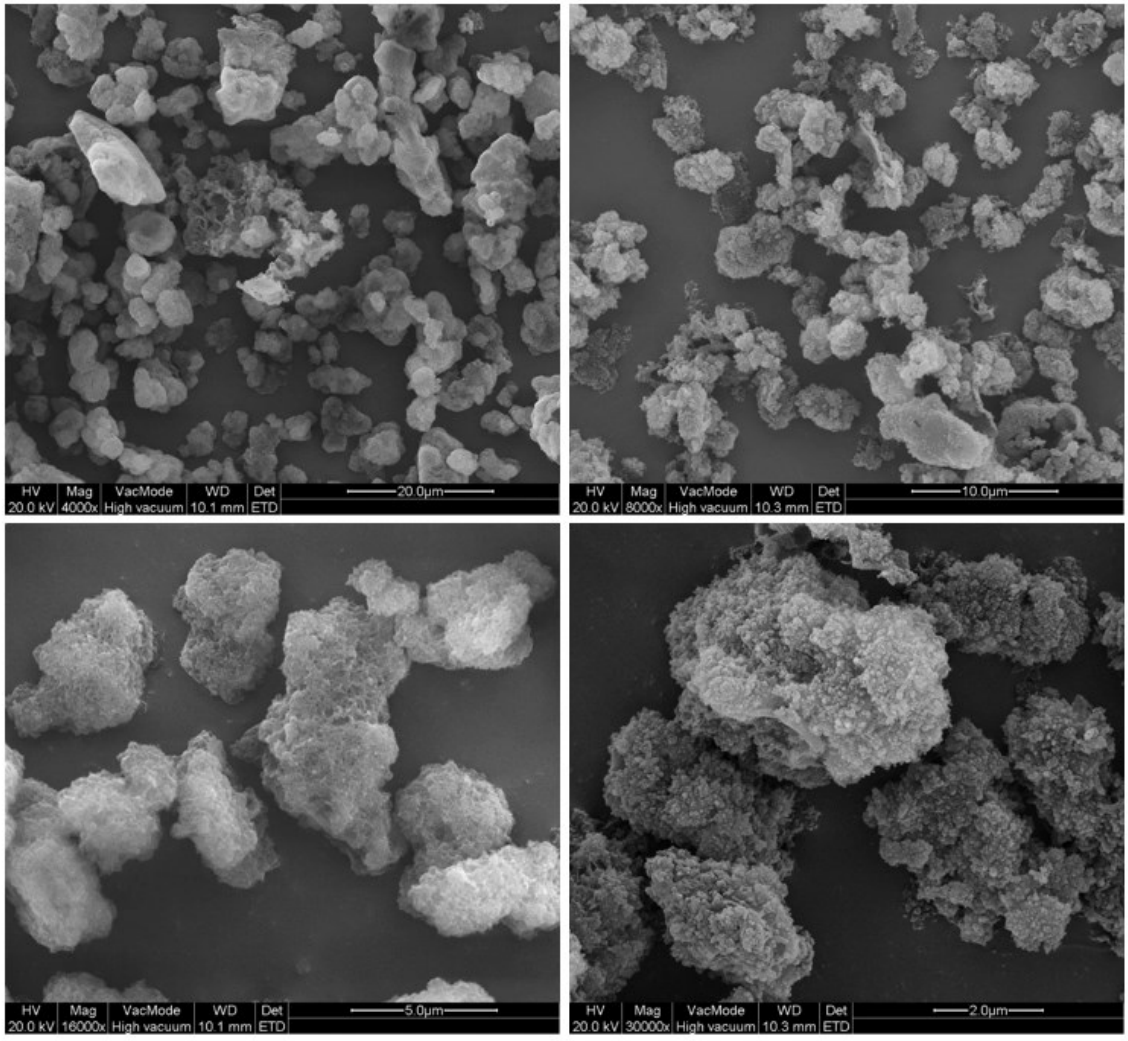

Figure S1. SEM image of Bipy-CTF presented at different magnifications.

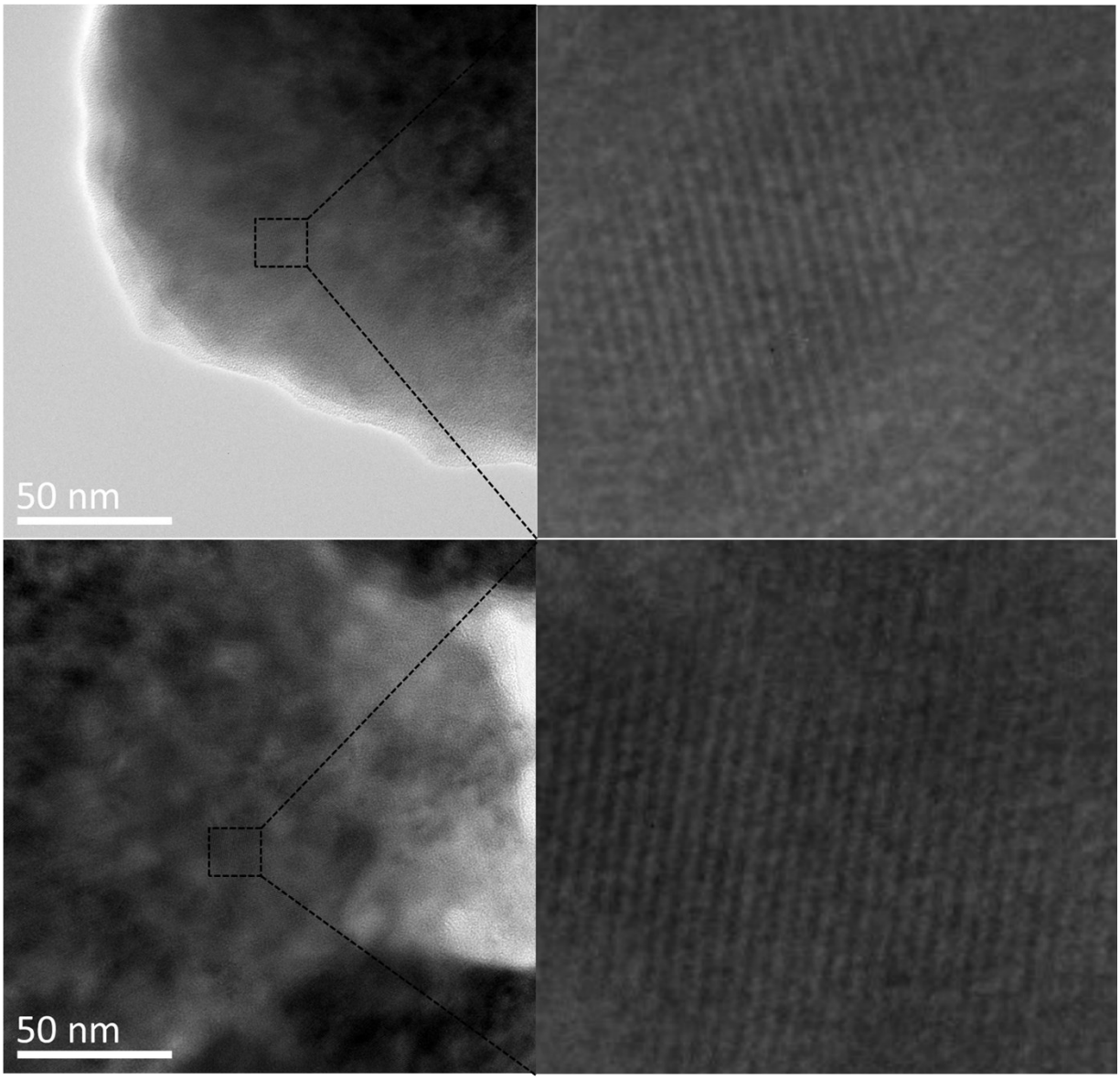

Figure S2. TEM image and higher-magnification HR-TEM image of Bipy-CTF.

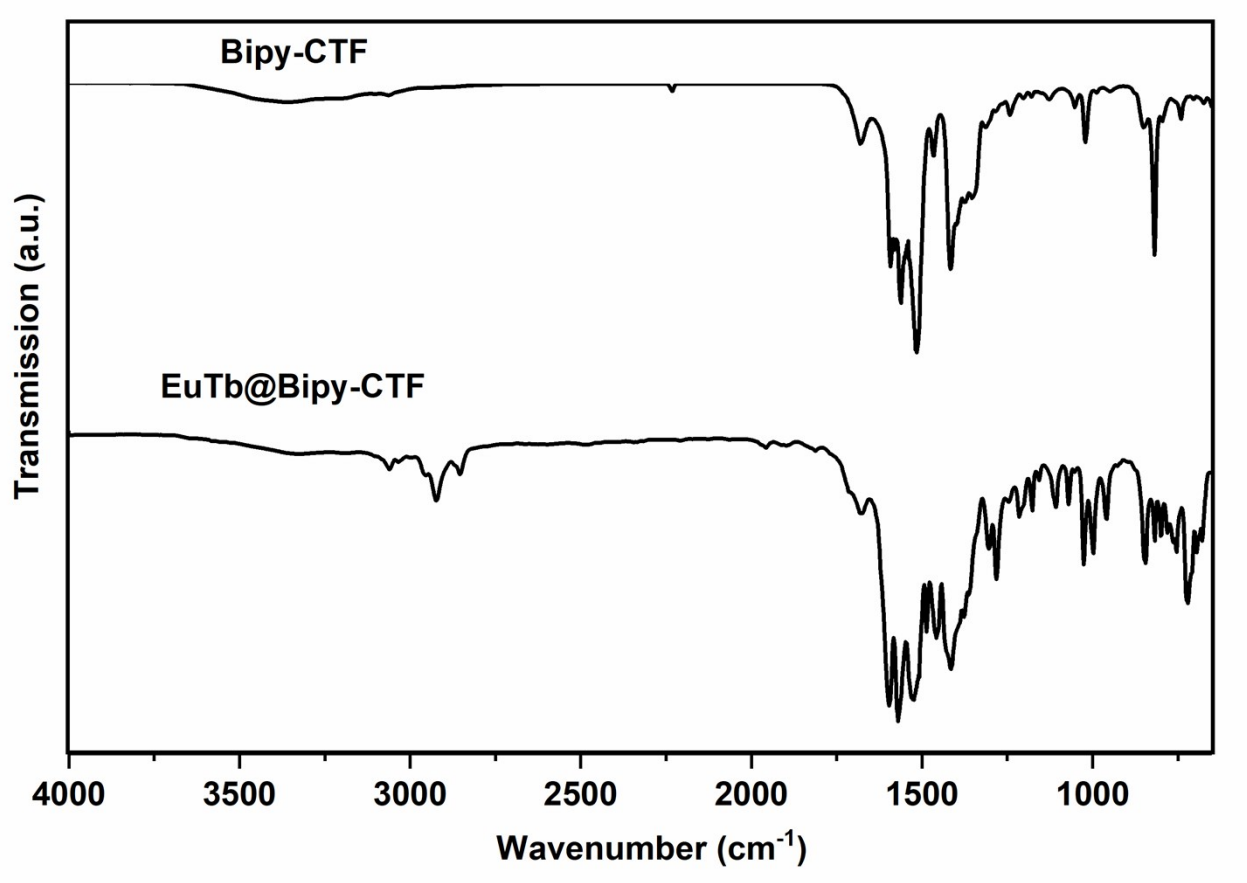

Figure S3. DRIFT spectra of Bipy-CTF and EuTb@BipyCTF.

Table S1. Elemental analysis of Bipy-CTF

Sample	Cal.			Exp.		
	N%	C%	H%	N%	C%	H%
Bipy-CTF	25.9	71.0	3.1	20.87	64.11	3.40

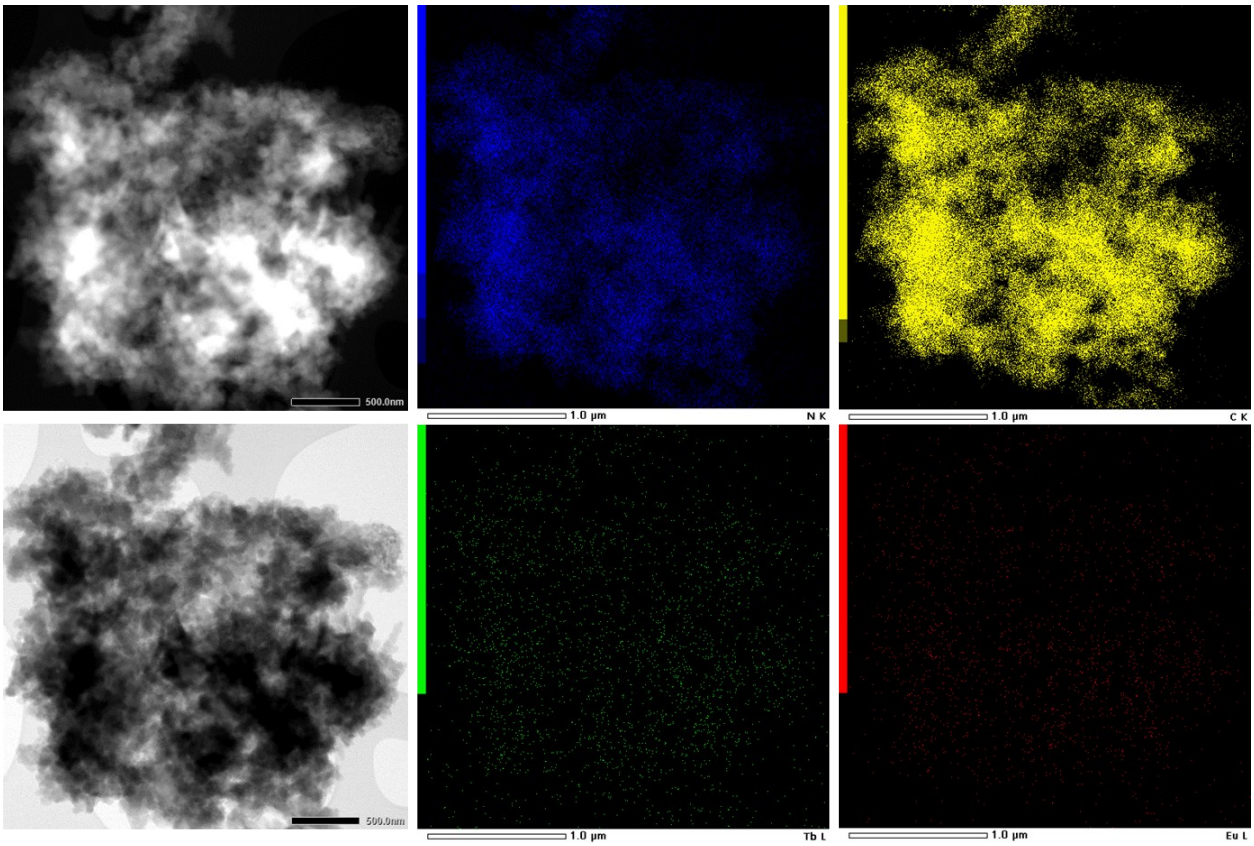

Figure S4. Dark-field TEM image of EuTb@Bipy-CTF and corresponding EDX elemental mapping of Eu (red) and Tb (green).

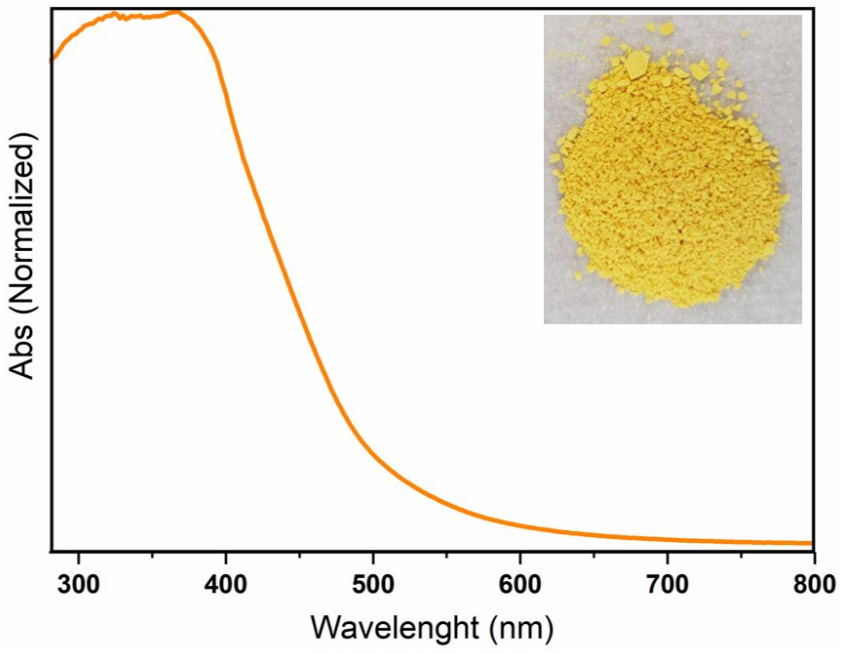

Figure S5. UV-Visible spectra and photo of the pristine Bipy-CTF.

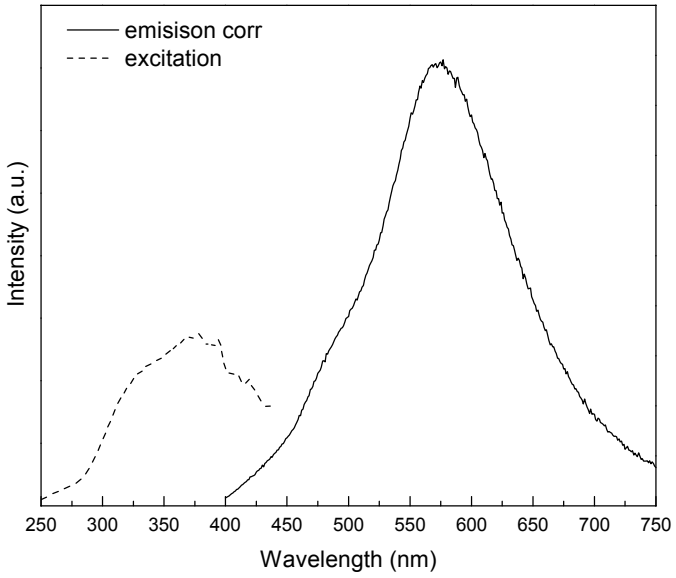

Figure S6. Combined excitation-emission spectrum of the pristine Bipy-CTF.

Table S2. Assignment of peaks for compound **1**

	Wavelength (nm)	Transitions
	excitation	
a	377.0	$\pi \rightarrow \pi^*$
	emission	
b	490.0	$^5D_4 \rightarrow {}^7F_6$
c	549.0	$^5D_4 \rightarrow {}^7F_5$
d	580.0	$^5D_4 \rightarrow {}^7F_4$
e	619.0	$^5D_4 \rightarrow {}^7F_3$

Table S3. Assignment of peaks for compound **2**

	Wavelength (nm)	Transitions
	excitation	
a	354.0	$\pi \rightarrow \pi^*$
b	395.0	$^5L_6 \leftarrow {}^7F_0$
	emission	
c	579.0	$^5D_0 \rightarrow {}^7F_0$
d	594.0	$^5D_0 \rightarrow {}^7F_1$
e	612.0	$^5D_0 \rightarrow {}^7F_2$
f	651.0	$^5D_0 \rightarrow {}^7F_3$
g	700.0	$^5D_0 \rightarrow {}^7F_4$

Table S4. Assignment of peaks for compound **3**

	Wavelength (nm)	Transitions
	excitation	
	327.0	$\pi \rightarrow \pi^*$
	emission	
a	489.0	$^5D_4 \rightarrow {}^7F_6$ (Tb)
b	549.0	$^5D_4 \rightarrow {}^7F_5$ (Tb)
c	579.0	$^5D_4 \rightarrow {}^7F_4$ (Tb)
d	593.0	$^5D_0 \rightarrow {}^7F_1$ (Eu)
e	610.0	$^5D_0 \rightarrow {}^7F_2$ (Eu)
f	652.0	$^5D_0 \rightarrow {}^7F_3$ (Eu)
g	704.0	$^5D_0 \rightarrow {}^7F_4$ (Eu)

Table S5. Assignment of peaks for compound **4**

	Wavelength (nm)	Transitions
	excitation	
a	378.0	$\pi \rightarrow \pi^*$
	emission	
b	491.0	$^5D_4 \rightarrow {}^7F_6$ (Tb)
c	549.0	$^5D_4 \rightarrow {}^7F_5$ (Tb)
d	580.0	$^5D_4 \rightarrow {}^7F_4$ (Tb)
e	590.0	$^5D_0 \rightarrow {}^7F_1$ (Eu)
f	610.0	$^5D_0 \rightarrow {}^7F_2$ (Eu)
g	651.0	$^5D_0 \rightarrow {}^7F_3$ (Eu)
h	703.0	$^5D_0 \rightarrow {}^7F_4$ (Eu)

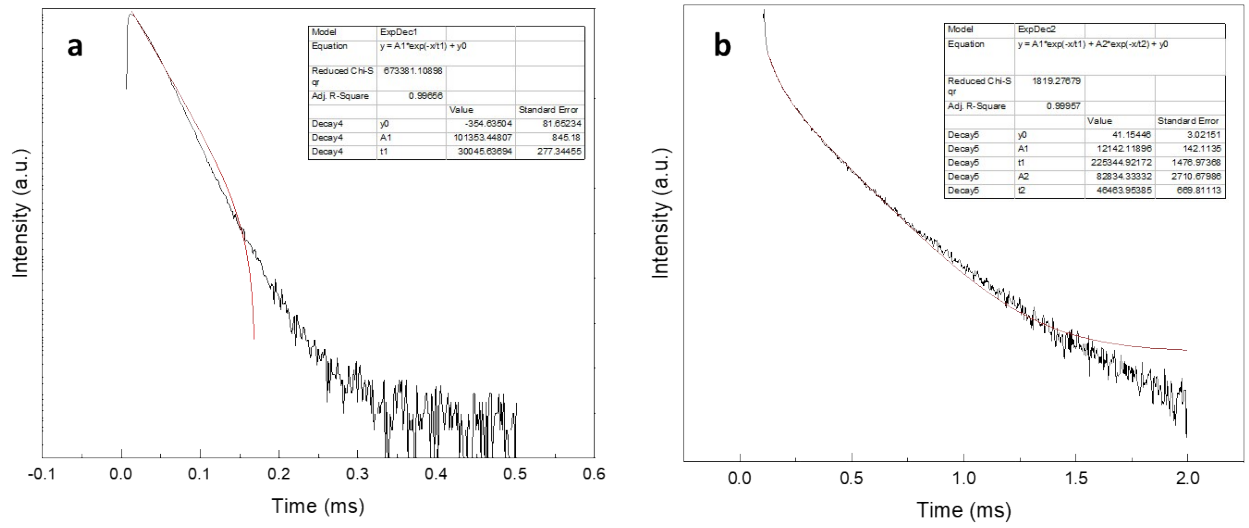

Figure S7. a) Decay profile of sample **1** recorded at RT. b) Decay profile of sample **2** recorded at RT.

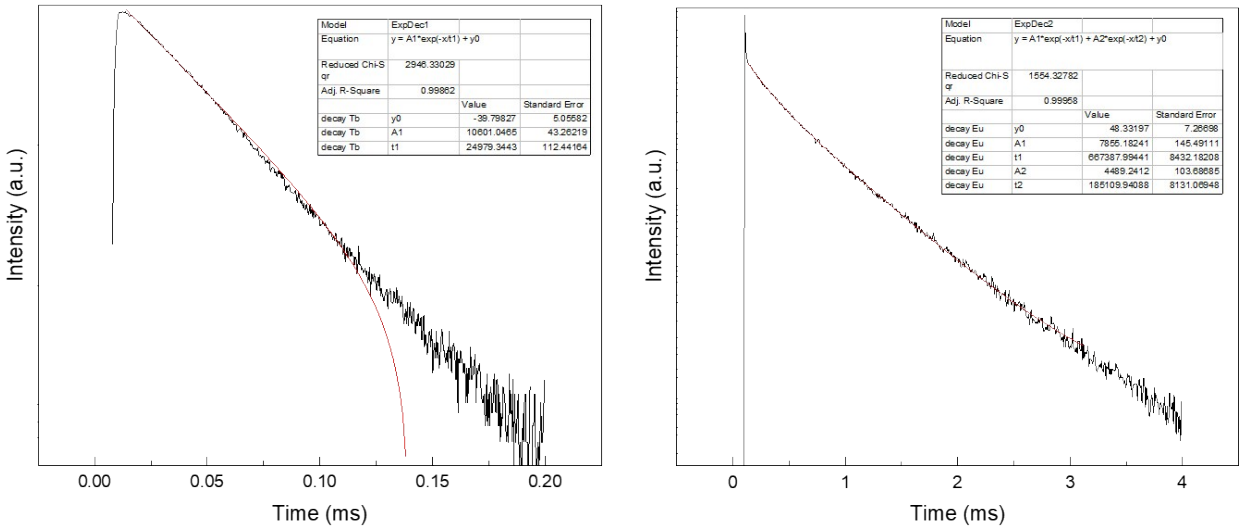

Figure S8. Decay profile of **3** recorded at RT (right recorded when observing Tb^{3+}, left recorded when observing Eu^{3+}).

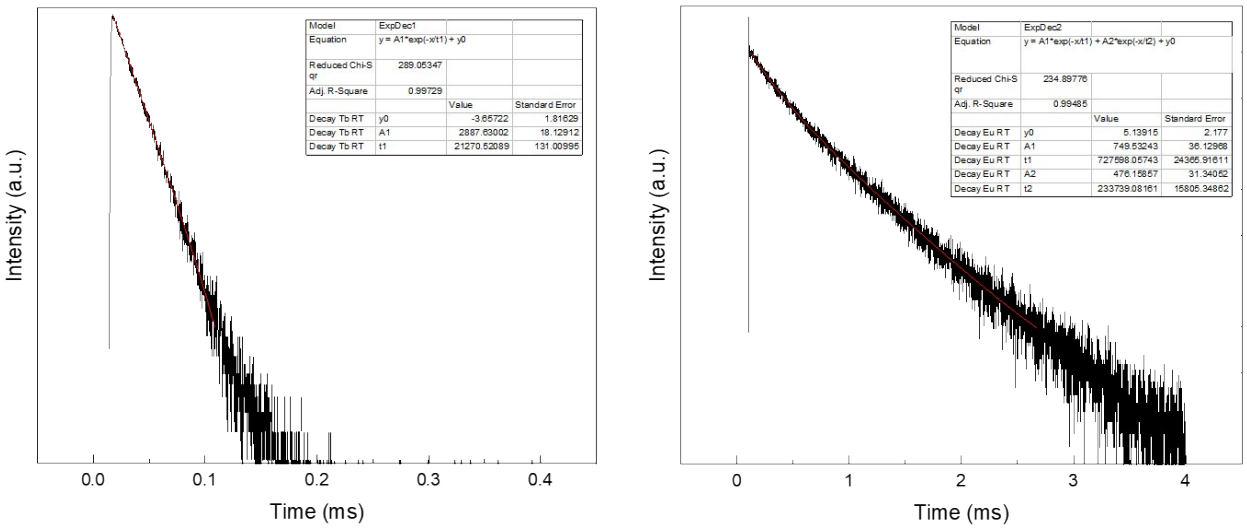

Figure S9. Decay profile of **4** recorded at RT (right recorded when observing Tb^{3+}, left recorded when observing Eu^{3+}).

Table S6. Luminescence decay time of Eu@Bipy-CTF, Tb@Bipy-CTF and EuTb@Bipy-CTF materials.

Sample	τ_1 (μs)/%	τ_2 (μs)/%	τ_{av} (μs)
Tb@Bipy-CTF (**1**)	30/100	-	-
Eu@Bipy-CTF(**2**)	225/13	46/87	120
3%Eu,97%Tb@Bipy-CTF(**3**) (observed Tb^{3+})	25/100	-	-
3%Eu,97%Tb@Bipy-CTF(**3**) (observed Eu^{3+})	667/64	185/36	608
5%Eu,95%Tb@Bipy-CTF(**4**) (observed Tb^{3+})	21/100	-	
5%Eu,95%Tb@Bipy-CTF(**4**) (observed Eu^{3+})	728/61	234/39	644

Note: average decay time calculated according to equation: $\tau_{av} = \frac{A_1\tau_f^2 + A_2\tau_s^2}{A_1\tau_f + A_2\tau_s}$ where τ_f is the fast decay time and τ_s is the slow decay time.

As can be seen from Table S6, the (average) decay times observed at 611.0 nm (Eu^{3+}) in materials **3** and **4** are longer compared to material **2**. However, the (average) decay times of materials **3** and **4** observed at 544.0 nm (Tb^{3+}) are shorter than that of material **1**. This would indicate that in the EuTb@Bipy-CTF materials energy is transferred from the ligand to Tb^{3+} and then to Eu^{3+}.

For better understanding of the energy transfer mechanism in the material the triplet level in the Bipy-CTF grafted with $GdCl_3$ material has been determined at 77 K in ethanol/methanol mixture (4:1). The analysis is depicted in **Figure S10**. In gadolinium complexes, the energy at the triplet level of the ligand is not transferred to the Gd^{3+} metal, as the resonance level of Gd^{3+} lies far above the triplet level. Subsequently, we have recorded the decay time at its maximum and observed microsecond range lifetimes, confirming the band belongs to the triplet level of the material (**Figure S11**). The triplet level of Bipy-CTF grafted with $GdCl_3$ corresponds to the high-energy edge of this band, the lowest triplet level is therefore located at 460 nm (21740 cm^{-1}). The triplet level lies above the energy level of the $^5D_4$ accepting level of Tb^{3+} allowing successful energy transfer to Tb^{3+} and energy can further be transferred to the accepting levels of Eu^{3+}.

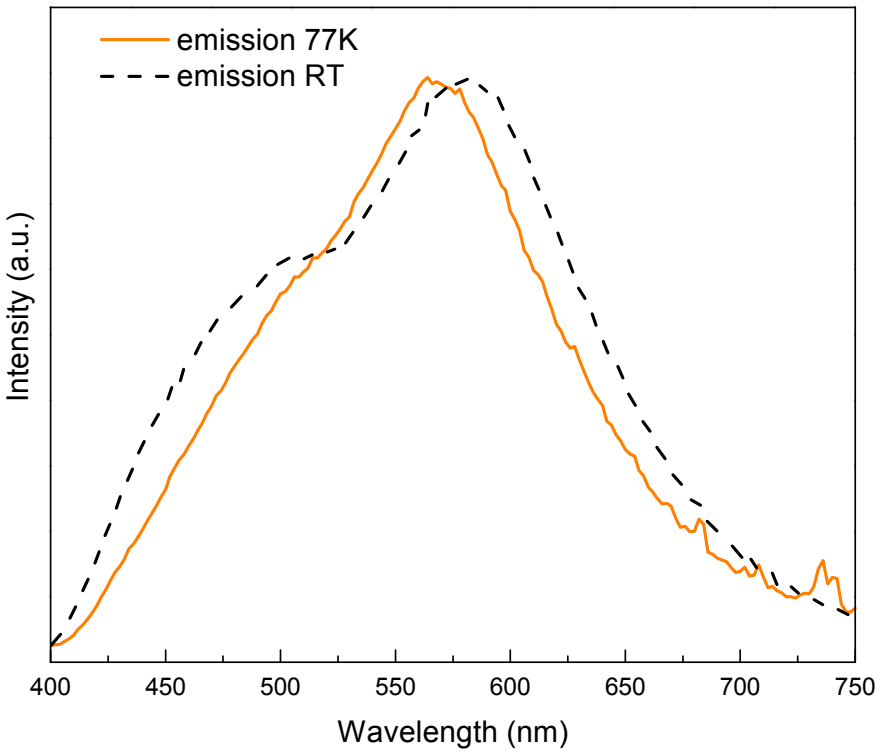

Figure S10. Emission spectra of Bipy-CTF grafted with $GdCl_3$, measured in ethanol: methanol (4:1) solution at RT and at 77 K.

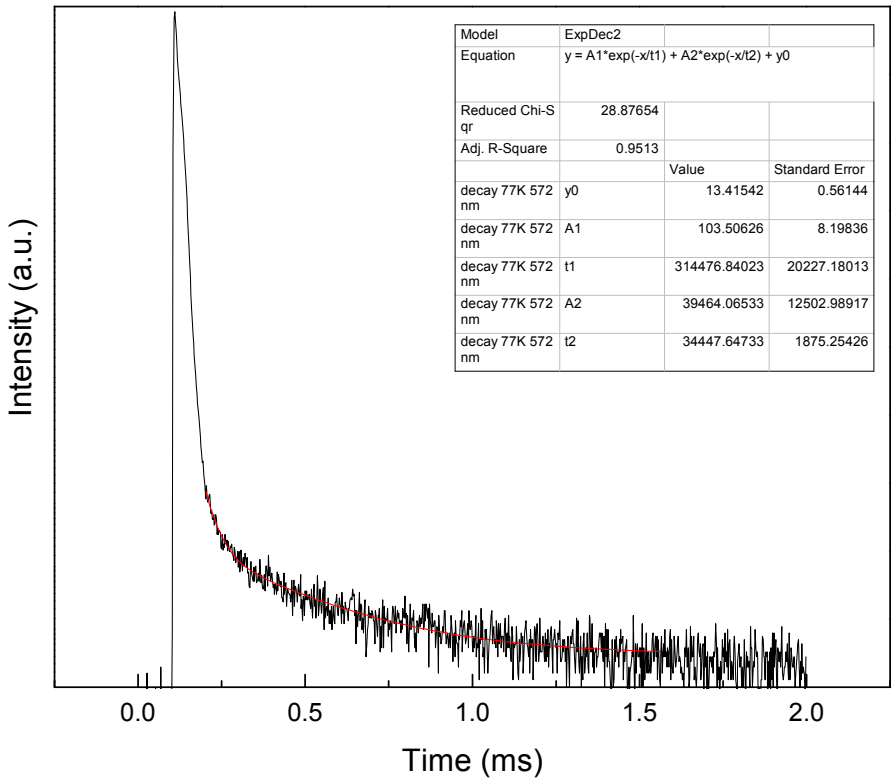

Figure S11. Decay time of Bipy-CTF grafted with $GdCl_3$, measured at 460 nm.

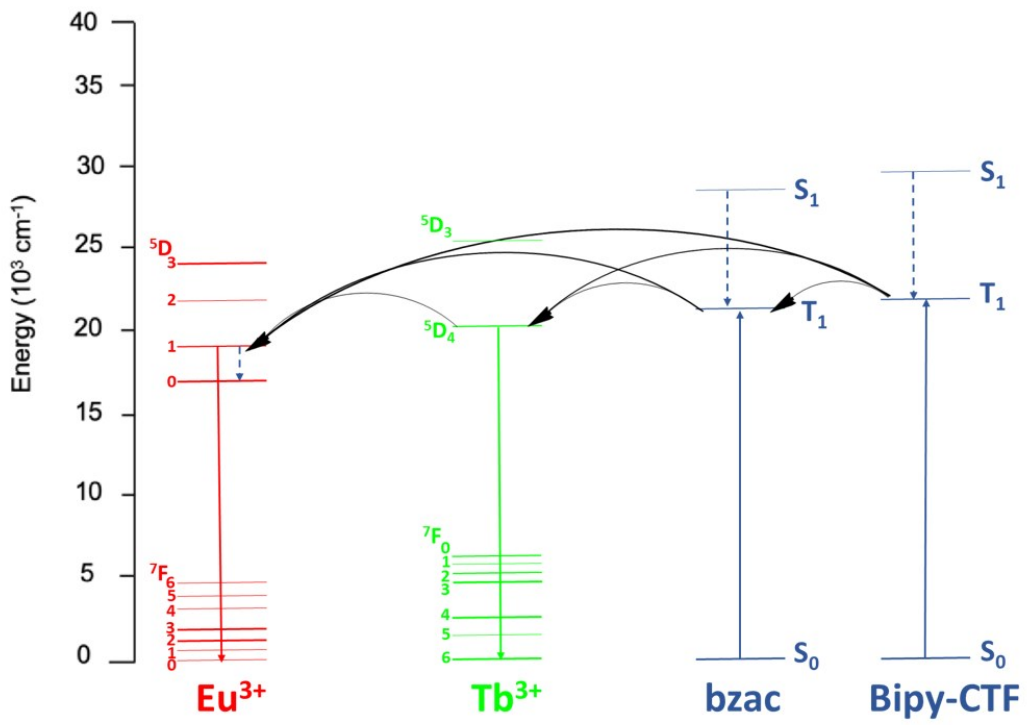

Scheme S1. Simplified visualization of the energy transfer mechanism in the EuTb@Bipy-CTF systems.

Table S7. An overview of the relative sensitivity Sr (highest value) for the reported luminescent thermometers (MOFs and coordination polymers) compared to the EuTb@BipyCTF materials (Entry 1 and 2) operating in physiological temperature range.

Entry	Materials	Temp. range [K]	Max. S_r [$\%K^{-1}$]	Ref.
1	Compound **3**	200-340	2.30 (240K)	This work
2	Compound **4**	253-333	2.12 (253K)	This work
3	ZJU-88⊃perylene	293-353	1.28 (293K)	2
4	$Tb_{0.99}Eu_{0.01}(BDC)_{1.5}(H_2O)_2$	298-320	0.14 (314 K)	3
5	$Tb_{0.7}Eu_{0.3}$L MOF	40 - 300	0.17 (300 K)	4
6	$(Eu_xTb_{1-x})_2(DMBDC)_3(H_2O)_4.DMF.H_2O$	10-300	1.3 (284 K)	5
7	$[(Tb_{0.914}Eu_{0.086})_2(PDA)_3(H_2O)]\cdot 2H_2O$	10-325	0.07 (325 K)	6
8	$Nd_{0.577}Yb_{0.423}BDC\text{-}F_4$	293-313	1.201 (313 K)	7
9	$Tb_{0.999}Eu_{0.001}$BPDC	100-300	1.23	8
10	EuTb@ In(OH)(bpydc)	283-333	4.97	9
11	$Tb_{0.9}Eu_{0.1}$PIA	10-300	3.53	10

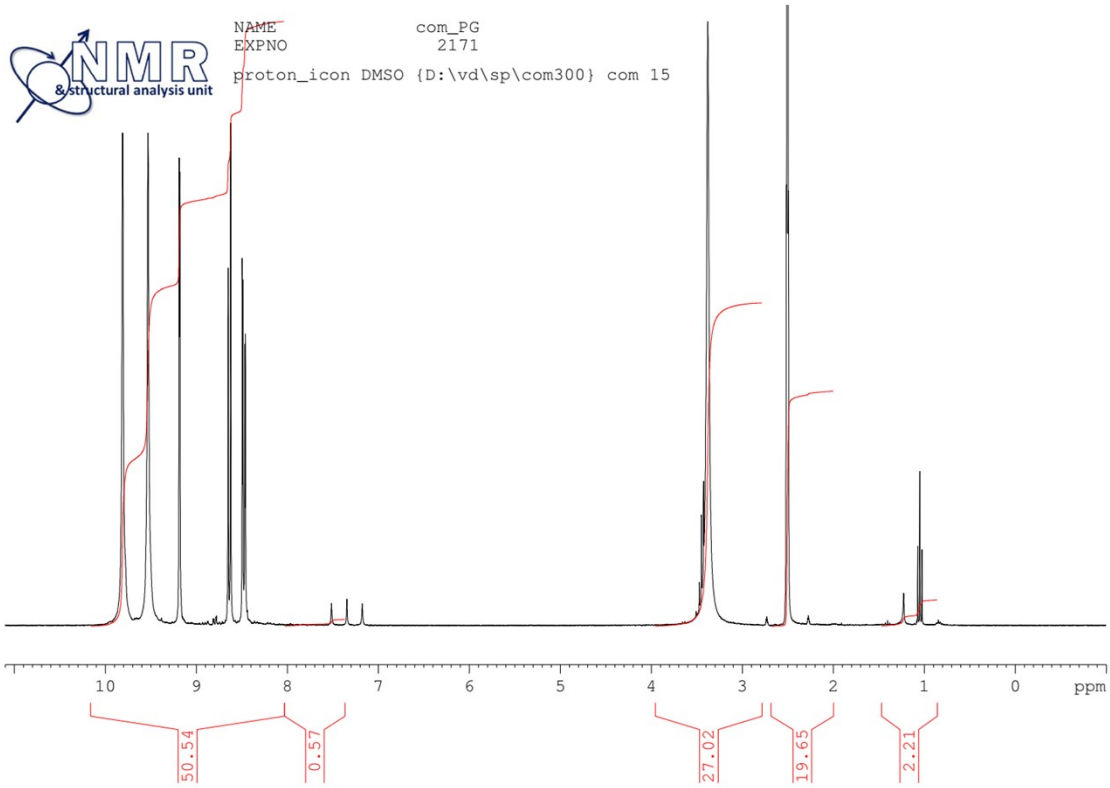

Figure S12. HNMR of 2,2'-bipyridine-5,5'-diamidine tetrahydrochloride

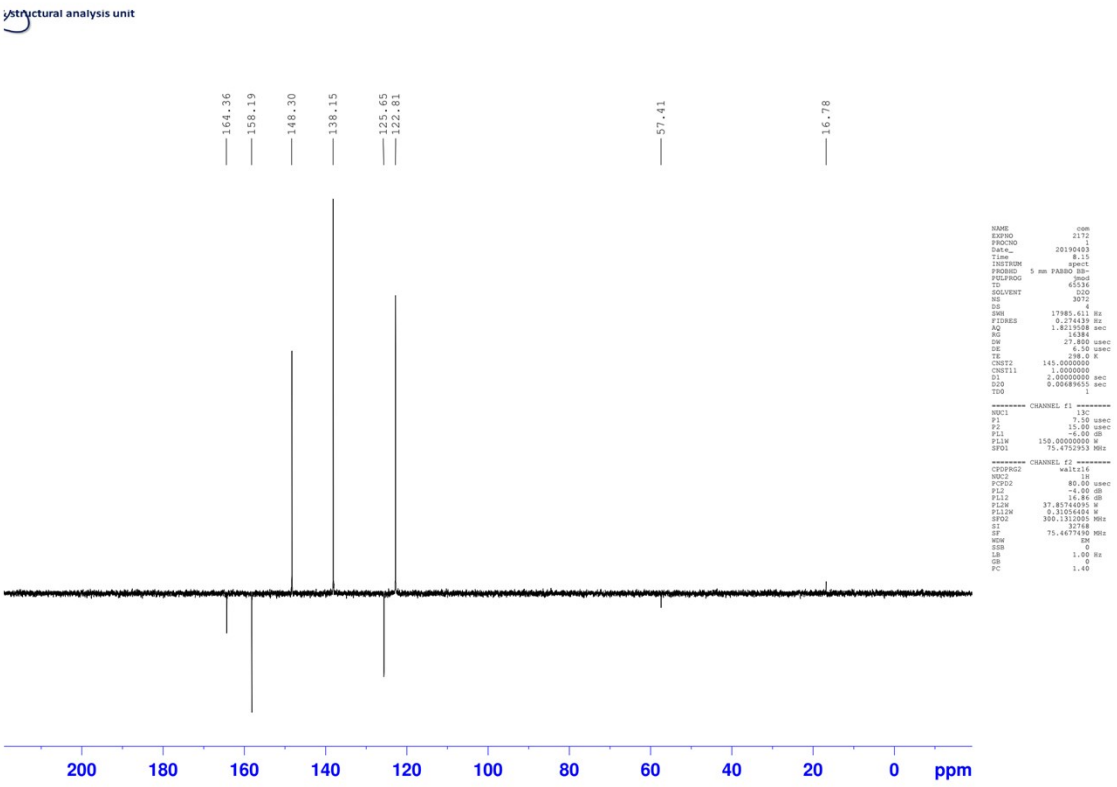

Figure S13. CNMR of 2,2'-bipyridine-5,5'-diamidine tetrahydrochloride

Computational modelling. A similar reported procedure was followed.[11] Theoretically, the condensation of [2,2'-bipyridine]-5,5'-bis(carboximidamide) and terephtaldehyde could lead to two different structures. Model 1 is characterized by a single-pore structure with each pore consisting of 4 bipyridine moieties and 2 phenyl moieties, Model 2 on the other hand possesses a dual-pore skeleton, with a central pore consisting of 6 bipyridine moieties being surrounded by 6 pores built from 3 bipyridine moieties and 3 phenyl moieties. To determine the correct structure of the CTF, theoretical PXRD patterns of both models were modelled using Materials Studio 2017 software. First a structure comparable to the ones shown in Scheme S1 was built (in P1 symmetry)

in Accelrys Materials Studio 17.1 (Biovia, San Diego, USA). Subsequently, the geometry, symmetry and unit cell parameters were optimized using the Forcite tool. Then the simulated PXRD patterns could be calculated using the Reflex module. Finally, the optimized structure was subjected to Pawley refinement (using the Reflex module), from 2 to 40° 2θ (λ=1.54Å). Fitting (U, V and W), profile (NA and NB), line shift (zero point, shift #1 and shift #2) and unit cell (a, b, c) parameters were allowed to vary freely during refinement. Peaks were fit using Pseudo-Voigt functions and background was modelled using a 20-order polynomial. Crystallite size or lattice strain broadening was not taken into account during refinement. To determine the correct structure of the Bipy-CTF, a theoretical PXRD pattern was modelled using Materials Studio 2017 software. Both eclipsed (AA) and staggered (AB) structures were generated (**Figure S14**) but based on the major differences between the experimental pattern and the AB modelled one, only the eclipsed structure was taken into consideration. Subsequently, the eclipsed structure was Pawley refined to the experimental data (both the raw and background corrected data were used, from 2 to 40° 2θ), obtaining an optimized structure assigned to the *C*mmm space group with optimized unit cell parameter of a = 30.91, b = 20.76 and c = 3.51 (for raw data) and a = 30.95, b = 20.79 and c = 3.50 when using background corrected data. With low R_{wp} and R_p values (6.69% and 5.24% respectively, for the raw data and 2.22% and 1.51% respectively for the background corrected data) and no visible deviations from the experimental pattern or significant peaks in the difference plot, this model proves to be a good fit. In **Figure S15** the Pawley refinement of the raw experimental pattern without background correction is presented.

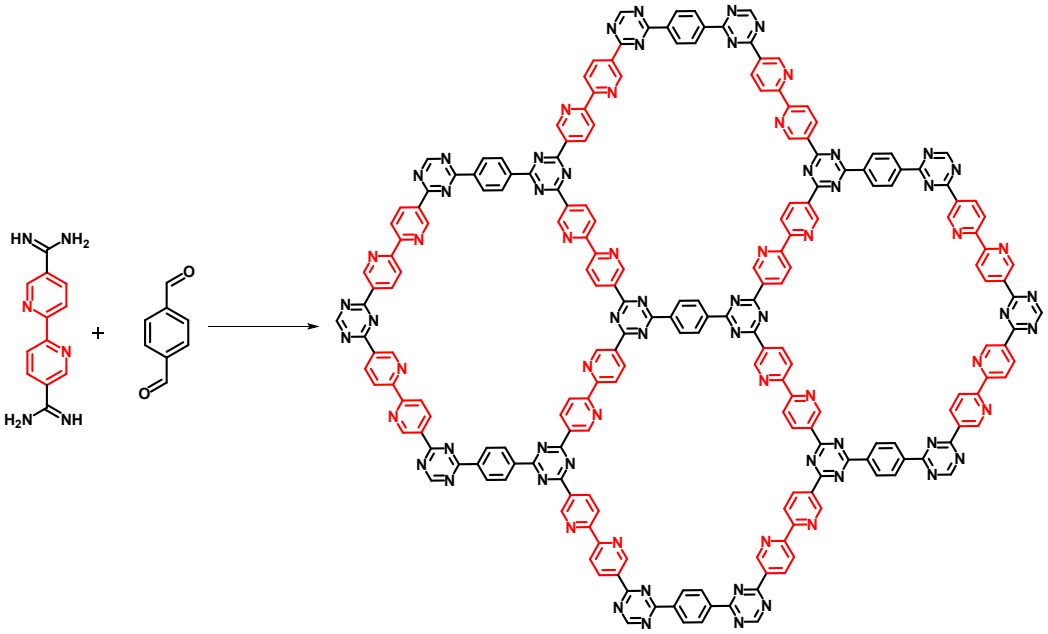

Scheme S1. The possible framework of condensation of [2,2'-bipyridine]-5,5' bis(carboximidamide) and terephtaldehyde.

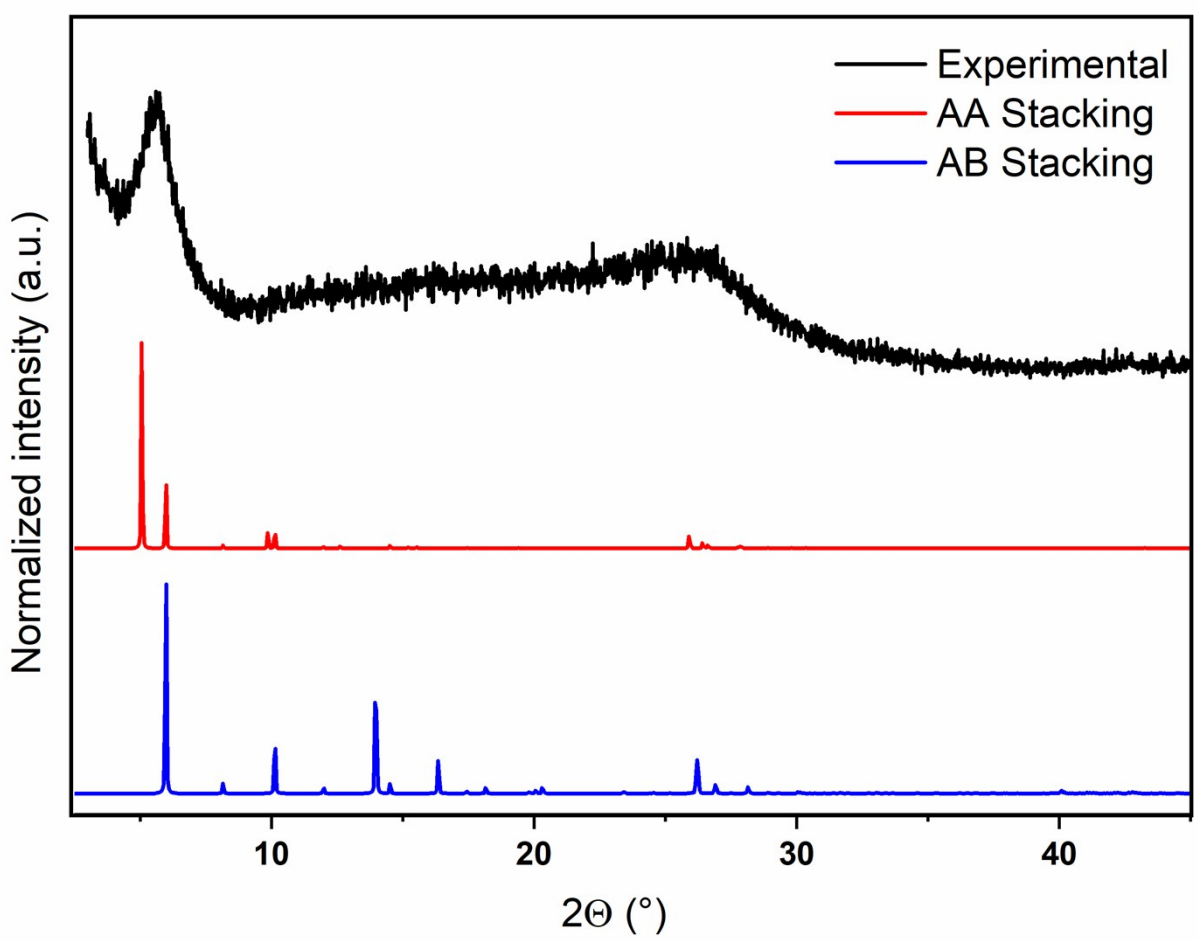

Figure S14.The normalized experimental PXRD pattern (black) compared to the normalized modelled stacking modes for Bipy-CTF (red for AA stacking, blue for AB stacking).

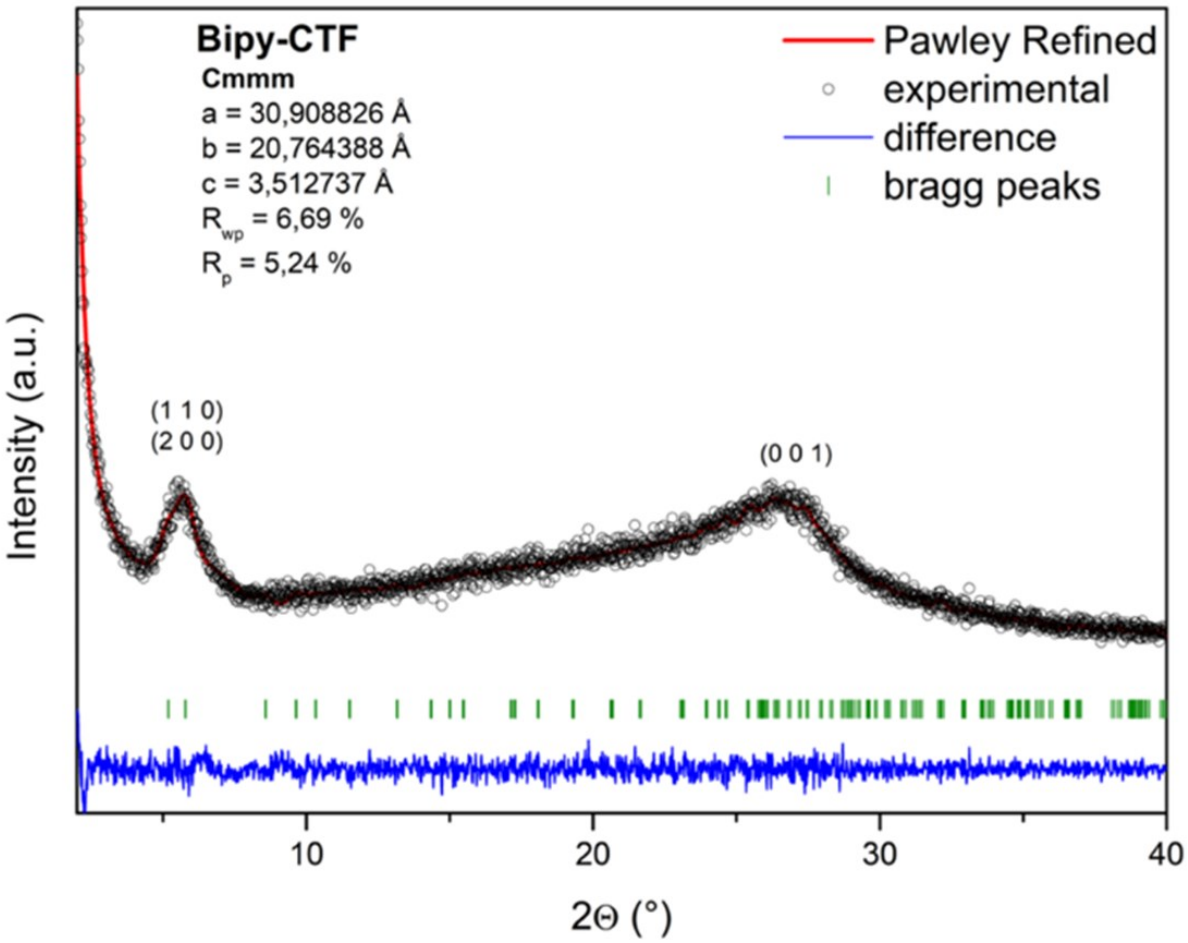

Figure S15. Experimental (black) and Pawley refined (red) PXRD patterns of modelled Bipy CTF, accompanied with the difference plot (blue) and Bragg peak positions (green) of the corresponding model.

References

1. Kaczmarek, A. M.; Van Deun, R.; Kaczmarek, M. K., TeSen - tool for determining thermometric parameters in ratiometric optical thermometry. *Sensor Actuat B-Chem* **2018,** *273*, 696-702.

2. Cui, Y. J.; Song, R. J.; Yu, J. C.; Liu, M.; Wang, Z. Q.; Wu, C. D.; Yang, Y.; Wang, Z. Y.; Chen, B. L.; Qian, G. D., Dual-Emitting MOF superset of Dye Composite for Ratiometric Temperature Sensing. *Adv Mater* **2015,** *27* (8), 1420-+.

3. Cadiau, A.; Brites, C. D. S.; Costa, P. M. F. J.; Ferreira, R. A. S.; Rocha, J.; Carlos, L. D., Ratiometric Nanothermometer Based on an Emissive Ln(3+)-Organic Framework. *Acs Nano* **2013,** *7* (8), 7213-7218.

4. Zhao, S. N.; Li, L. J.; Song, X. Z.; Zhu, M.; Hao, Z. M.; Meng, X.; Wu, L. L.; Feng, J.; Song, S. Y.; Wang, C.; Zhang, H. J., Lanthanide Ion Codoped Emitters for Tailoring Emission Trajectory and Temperature Sensing. *Adv Funct Mater* **2015,** *25* (9), 1463-1469.

5. Cui, Y. J.; Xu, H.; Yue, Y. F.; Guo, Z. Y.; Yu, J. C.; Chen, Z. X.; Gao, J. K.; Yang, Y.; Qian, G. D.; Chen, B. L., A Luminescent Mixed-Lanthanide Metal-Organic Framework Thermometer. *J Am Chem Soc* **2012,** *134* (9), 3979-3982.

6. Wang, Z. P.; Ananias, D.; Carne-Sanchez, A.; Brites, C. D. S.; Imaz, I.; Maspoch, D.; Rocha, J.; Carlos, L. D., Lanthanide-Organic Framework Nanothermometers Prepared by Spray-Drying. *Adv Funct Mater* **2015,** *25* (19), 2824-2830.

7. Lian, X. S.; Zhao, D.; Cui, Y. J.; Yang, Y.; Qian, G. D., A near infrared luminescent metal-organic framework for temperature sensing in the physiological range. *Chem Commun* **2015,** *51* (100), 17676-17679.

8. Shen, X.; Lu, Y.; Yan, B., Lanthanide Complex Hybrid System for Fluorescent Sensing as Thermometer. *Eur J Inorg Chem* **2015,** (6), 916-919.

9. Zhou, Y.; Yan, B.; Lei, F., Postsynthetic lanthanide functionalization of nanosized metal-organic frameworks for highly sensitive ratiometric luminescent thermometry. *Chem Commun* **2014,** *50* (96), 15235-15238.

10. Rao, X. T.; Song, T.; Gao, J. K.; Cui, Y. J.; Yang, Y.; Wu, C. D.; Chen, B. L.; Qian, G. D., A Highly Sensitive Mixed Lanthanide Metal-Organic Framework Self-Calibrated Luminescent Thermometer. *J Am Chem Soc* **2013,** *135* (41), 15559-15564.

11. Feldblyum, J. I.; McCreery, C. H.; Andrews, S. C.; Kurosawa, T.; Santos, E. J. G.; Duong, V.; Fang, L.; Ayzner, A. L.; Bao, Z. N., Few-layer, large-area, 2D covalent organic framework semiconductor thin films. *Chem Commun* **2015,** *51* (73), 13894-13897.